Materials **2013**, *6*, 1621-1631; doi:10.3390/ma6051621

OPEN ACCESS

materials

ISSN 1996-1944

www.mdpi.com/journal/materials

Article

The Effect of PtRuIr Nanoparticle Crystallinity in Electrocatalytic Methanol Oxidation

Yanjiao Ma [1], Rongfang Wang [1,*], Hui Wang [1], Shijun Liao [2], Julian Key [3], Vladimir Linkov [3] and Shan Ji [3,*]

[1] Key Laboratory of Eco-Environment-Related Polymer Materials of Ministry of Education of China, College of Chemistry and Chemical Engineering, Northwest Normal University, Lanzhou 730070, China; E-Mails: myjmm@126.com (Y.M.); wanghui3931@126.com (H.W.)

[2] Key Laboratory of Fuel Cell Technology of Guangdong Province, South China University of Technology, Guangdong, Guangzhou 510640, China; E-Mail: chsjliao@scut.edu.cn

[3] South African Institute for Advanced Materials Chemistry, University of the Western Cape, Cape Town 7535, South Africa; E-Mails: joolskey@yahoo.com (J.K.); vlinkov@uwc.ac.za (V.L.)

* Author to whom correspondence should be addressed; E-Mails: wrf38745779@126.com (R.W.); sji@uwc.ac.za (S.J.); Tel./Fax: +86-931-797-1533 (R.W.); +27-21-959-9316 (S.J.).

Received: 18 February 2013; in revised form: 23 April 2013 / Accepted: 24 April 2013 / Published: 29 April 2013

Abstract: Two structural forms of a ternary alloy PtRuIr/C catalyst, one amorphous and one highly crystalline, were synthesized and compared to determine the effect of their respective structures on their activity and stability as anodic catalysts in methanol oxidation. Characterization techniques included TEM, XRD, and EDX. Electrochemical analysis using a glassy carbon disk electrode for cyclic voltammogram and chronoamperometry were tested in a solution of 0.5 mol L^{-1} CH_3OH and 0.5 mol L^{-1} H_2SO_4. Amorphous PtRuIr/C catalyst was found to have a larger electrochemical surface area, while the crystalline PtRuIr/C catalyst had both a higher activity in methanol oxidation and increased CO poisoning rate. Crystallinity of the active alloy nanoparticles has a big impact on both methanol oxidation activity and in the CO poisoning rate.

Keywords: electrocatalysts; fuel cells; methanol oxidation; structure; crystallinity

1. Introduction

Increasing the electrocatalytic activity and stability of Pt-based catalysts has been the focus of much recent research [1–3] and remains a critical requirement for the future implementation of direct methanol fuel cells (DMFCs). Among the various Pt-based binary catalysts, the PtRu alloy has been reported as the most effective for methanol electro-oxidation [4–6], with further recent gains in activity and durability reported by incorporating a third metal, such as Co, Ni, Sn, Ir, *etc.* [7–10]. Among these ternary alloy catalysts, the PtRuIr/C system seems particularly promising [11–13]. Furthermore, the effect of composition for PtRuIr/C catalyst was systematically studied. However, the effect of its structure and morphology on methanol electro-oxidation is not focused on by other researchers.

Synthesis of nanostructured electrocatalysts is of great importance in developing the so-called "next-generation" catalysts [14]. The catalytic activity of such nanostructured electrocatalysts is highly dependent on the surface area, surface atomic structure, crystal size and shape. With control of nanostructure and morphology, large surface areas and abundant catalytic active sites can be realized, which enhance catalytic performance and utilization efficiency of the electrocatalyst [15]. In particular, amorphous structures in alloys can present unique compositions and catalytic surface structures as compared to conventional crystallized metal [16,17]. Some studies show that amorphous composition can have positive effects on the kinetics or stability of the methanol oxidation reaction due to amorphous alloys presenting unique compositions and surface structures for molecular reactions [18], while others show that intermetallic compounds with high-crystallinity have higher electrocatalytic activity for methanol oxidation reaction [19,20].

Inspired by the reports, the present work aimed to gain deeper insight into the effect of PtRuIr nanoparticle crystallinity on methanol electro-oxidation for carbon-supported PtRuIr catalysts. To this end, crystalline and amorphous carbon-supported PtRuIr structures were prepared, and then studied and compared using cyclic voltammetry and chronoamperometry.

2. Results and Discussion

X-Ray Diffraction (XRD) analysis (Figure 1) produced clear differences in the peak distributions of the carbon-supported $PtRuIr_c/C$ (crystalline form) and $PtRuIr_a/C$ (amorphous form) catalysts. In the diffractograms of the two catalysts, the first peak located at about 24.8° in all the XRD plots is associated with the Vulcan XC-72R support, and no peaks corresponding to the metals Ir and Ru were observed [11]. For clarity, the diffraction patterns of the $PtRuIr_a/C$ catalyst between 32° and 70° have been enlarged in the inset of Figure 1. Here, the $PtRuIr_a/C$ catalyst had only one wide, diffuse, broad peak at approximately $2\theta = 45°$, indicating that the sample's internal structure was amorphous [18]. In contrast, the XRD pattern of the heat treated sample, $PtRuIr_c/C$, have the five main characteristic peaks of the face-centered cubic (fcc) crystalline Pt alloy [13,21,22], corresponding to the planes (111), (200), (220), (311), and (222), at 2θ values of *ca.* 40°, 47°, 68°, 82°and 86°, respectively. On the other hand, a displacement of the peaks related to the polycrystalline Pt towards more positive values of 2θ is observed. This can be ascribed to the existence of alloys between the metals Pt, Ru and Ir. The formation of alloy results in a contraction of the crystalline lattice of Pt due to the substitution of some atoms of Pt with large size (r_{Pt} = 0.138 nm) for the atoms of Ir and/or Ru with small sizes

(r_{Ru} = 0.134 nm) (r_{Ir} = 0.136 nm) [11,23]. These results indicate that the $PtRuIr_c$ alloy supported on carbon catalyst had fcc crystalline structure.

Figure 1. X-Ray Diffraction (XRD) patterns of $PtRuIr_c/C$ and $PtRuIr_a/C$ catalysts.

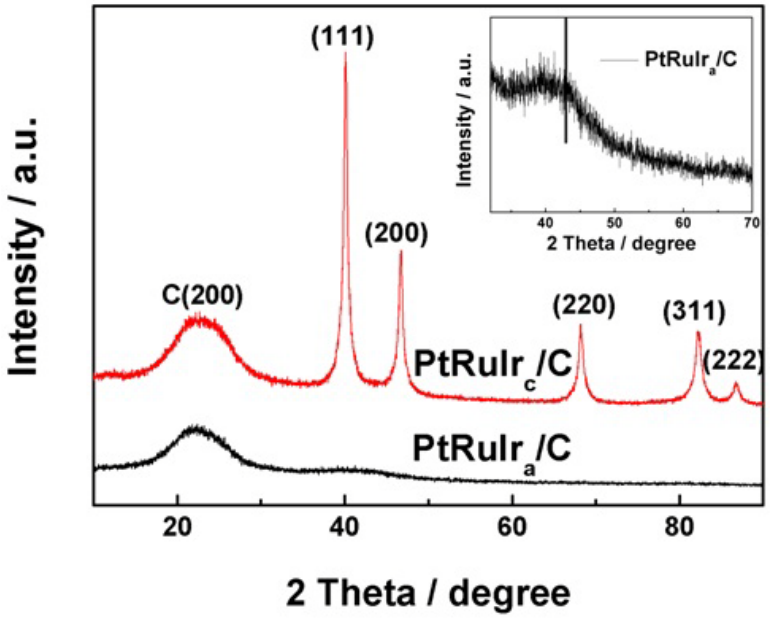

Figure 2 shows TEM images, corresponding particle sizes distribution histogram and EDX composition of $PtRuIr_a/C$ and $PtRuIr_c/C$. From the Figure 2A ($PtRuIr_a/C$) and 2B ($PtRuIr_c/C$), it can be observed that both catalysts were highly dispersed on the carbon support. The particle size distribution histogram of $PtRuIr_a/C$ (Figure 2C) and $PtRuIr_c/C$ (Figure 2D) catalyst based on examination of more than 300 particles show that the particle size varied from 1.0 to 4.5 nm for $PtRuIr_a/C$ and 3 to 9 nm for $PtRuIr_c/C$ and a relatively narrow size distribution for both catalysts. The derived average particle size is about 2.2 ± 0.02 nm and 5.0 ± 0.02 nm for the $PtRuIr_a/C$ and $PtRuIr_c/C$ catalysts (see Table 1), respectively. The HRTEM image of $PtRuIr_a/C$ in Figure 2E shows an inexplicit lattice, indicating that the particles of $PtRuIr_a/C$ are of mainly amorphous state [24]. In contrast, the HRTEM image (insets in Figure 2F) reveals that the $PtRuIr_c/C$ nanoparticles are crystalline, showing a lattice of ~0.23 nm identifiable as the d-spacing of the (111) plane of face-centered cubic Pt [25]. The EDS results of $PtRuIr_c/C$ and $PtRuIr_a/C$ (insets in Figure 2A,B) indicate that the both catalysts consist of: C, Pt, Ru and Ir, and *ca*. 3.5:3:1 of atom ratio for Pt:Ru:Ir is obtained. The result is also confirmed by ICP analysis. The metal loading for the two catalysts is *ca.* 20%, close to the normal value.

Typical cyclic voltammograms (CVs) of $PtRuIr_c/C$ and $PtRuIr_a/C$ catalysts in 0.5 mol L^{-1} H_2SO_4 solution are shown in Figure 3. A well-defined CV feature of polycrystalline Pt is observable in the curve generated from $PtRuIr_c/C$. Here, there are three pairs of redox peaks around 0.09, 0.173 and 0.214 V (*vs.* RHE), corresponding to the planes (110), (111), and (100), which can be ascribed to hydrogen adsorption/desorption on crystal surface sites of Pt [7,26]. In contrast, the CV curve of $PtRuIr_a/C$ catalyst only has one large, broad peak and does not exhibit the typical peaks of pure polycrystalline Pt between 0 and 0.3 V (*vs*. RHE). This further suggests that the active components of $PtRuIr_a/C$ catalyst had an amorphous structure. Furthermore, the oxide (OH_{ads}) stripping peak

(0.75 V *vs.* RHE) of the $PtRuIr_c/C$ is 70 mV more positive than that of $PtRuIr_a/C$ (0.68 V *vs.* RHE), suggesting faster hydroxyl desorption from the $PtRuIr_c/C$ surfaces [27].

Figure 2. TEM, the corresponding particle size distributing histogram and HRTEM images of $PtRuIr_a/C$ (**A**,**C**,**E**) and $PtRuIr_c/C$ (**B**,**D**,**F**) catalysts. Inset of (**A**) and (**B**): EDX spectrum of the $PtRuIr_a/C$ (**A**) and $PtRuIr_c/C$ (**B**) catalysts.

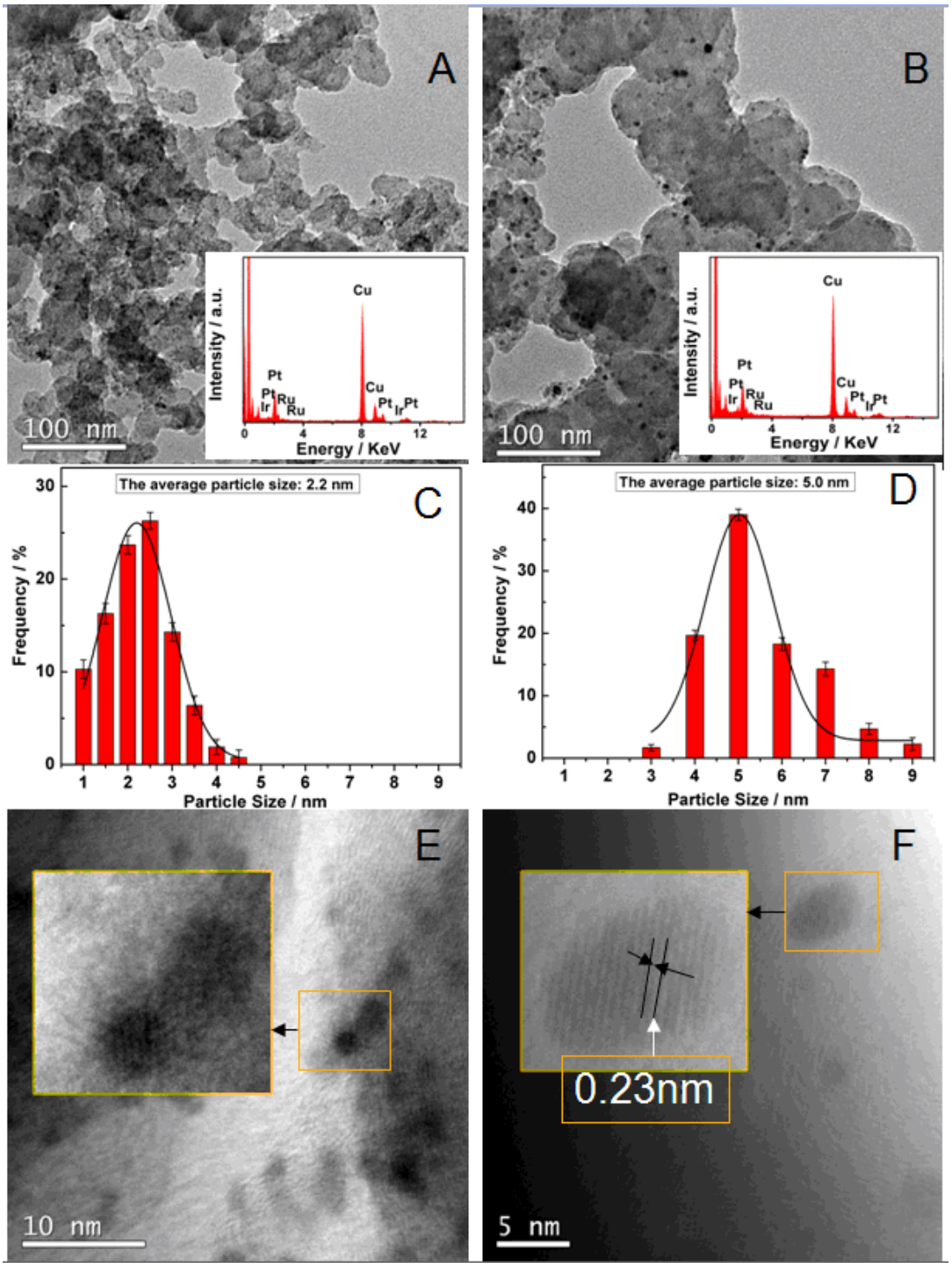

Table 1. Composition the average particle size, and the electrochemical performance of the $PtRuIr_a/C$ and $PtRuIr_c/C$ catalysts.

Catalyst	$PtRuIr_a/C$	$PtRuIr_c/C$
Pt:Ru:Ir atom ratio	3.5:3.0:1.0	3.5:3.0:1.0
The average particle size/nm	2.2 ± 0.02	5.0 ± 0.02
ECSA/$m^2\ g^{-1}_{metal}$	59.5	32.6
The onset potential for CO oxidation/mV *vs.* RHE	663	521
The onset potential for methanol oxidation/mV *vs.* RHE	370	338
The mass activity for methanol oxidation/mA mg^{-1}	147	298
The specific activity for methanol oxidation/mA cm^{-2}	0.25	0.91

Figure 3. Cyclic voltammograms of $PtRuIr_a/C$ and $PtRuIr_c/C$ catalysts in 0.5 mol L^{-1} H_2SO_4 solution under N_2 atmosphere; scan rate = 50 mV s^{-1}.

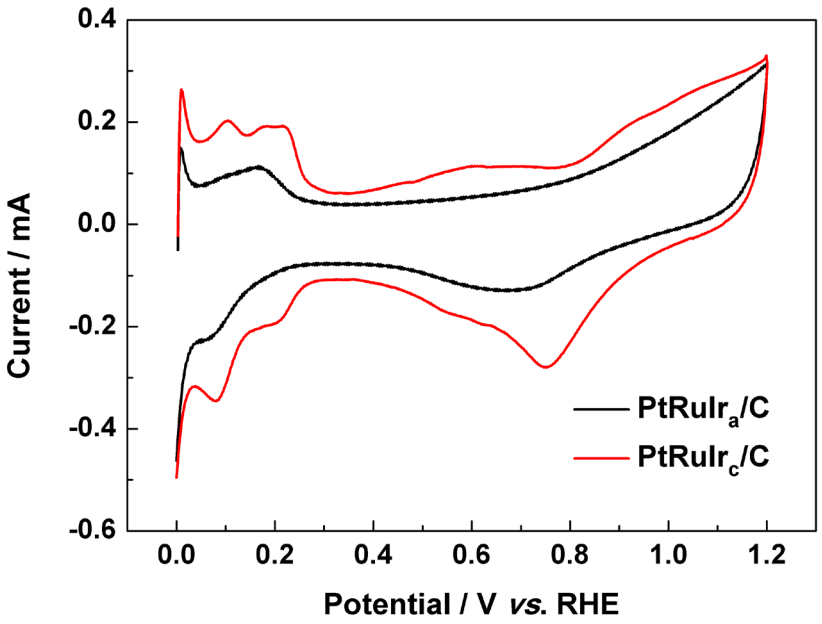

The CVs for CO electro-oxidation on $PtRuIr_c/C$ and $PtRuIr_a/C$ catalysts are shown in Figure 4. Here, the hydrogen desorption peaks were completely suppressed in the first scan in the lower potential region (0 to 0.3 *vs.* RHE), due to the saturated coverage of CO_{ads} species on the surface of PtRuIr alloy active sites [28]. However, hydrogen desorption peaks recovered in the second cycle after the CO was removed by oxidation.

It can be seen from Table 1 that the onset potential of CO electro-oxidation with $PtRuIr_c/C$ (0.54 V *vs.* RHE) is lower than that of $PtRuIr_a/C$ (0.67 V *vs.* RHE), which demonstrates that crystallinity of PtRuIr alloy influences the CO oxidation ability (the onset oxidation potential). The peak potential on the $PtRuIr_c/C$ catalyst (0.73 V *vs.* RHE) show a negative shift of around 0.45 V (*vs.* RHE) compared to the $PtRuIr_a/C$ catalyst (0.98 V *vs.* RHE). The lower peak potential and onset potential of the CO_{ads} oxidation on $PtRuIr_a/C$ indicate that $PtRuIr_c/C$ catalyst was kinetically more active for CO_{ads} oxidation [17]. The electrochemical surface area (*ECSA*) of the catalyst was calculated using the Equation (1) [29]:

$$ECSA_{CO} = \frac{Q_{CO}}{484\omega} \quad (1)$$

where Q_{CO} is the charge for CO desorption electro-oxidation in microcoulomb (μC), 484 is the charge required to oxidize a monolayer of CO on the catalyst in μC cm^{-2} and ω is the precious metal loading, respectively. The $ECSA_{CO}$ for $PtRuIr_c/C$ and $PtRuIr_a/C$ were 32.6 m^2 g^{-1}_{metal} and 59.5 m^2 g^{-1}_{metal} respectively. $PtRuIr_c/C$ had a lower $ECSA_{CO}$ than the $PtRuIr_a/C$.The real electrochemical surface area is determined by the active sites on the surface of the metal particle. The number of the active sites is related to the composition of the surface, the size of the particle and the structure of the surface [30]. After heat treatment, the $PtRuIr_c/C$ nanoparticles agglomerated resulting in increased particle size, which has been proved by TEM. The large particle size results in the small *ECSA* [31–33]. Therefore, we believe that the different $ECSA_{CO}$ mainly originated from the effect of particle size and structure.

Figure 4. CO stripping voltammograms of $PtRuIr_c/C$ and $PtRuIr_a/C$ catalysts in a solution of 0.5 mol L^{-1} H_2SO_4 at room temperature.

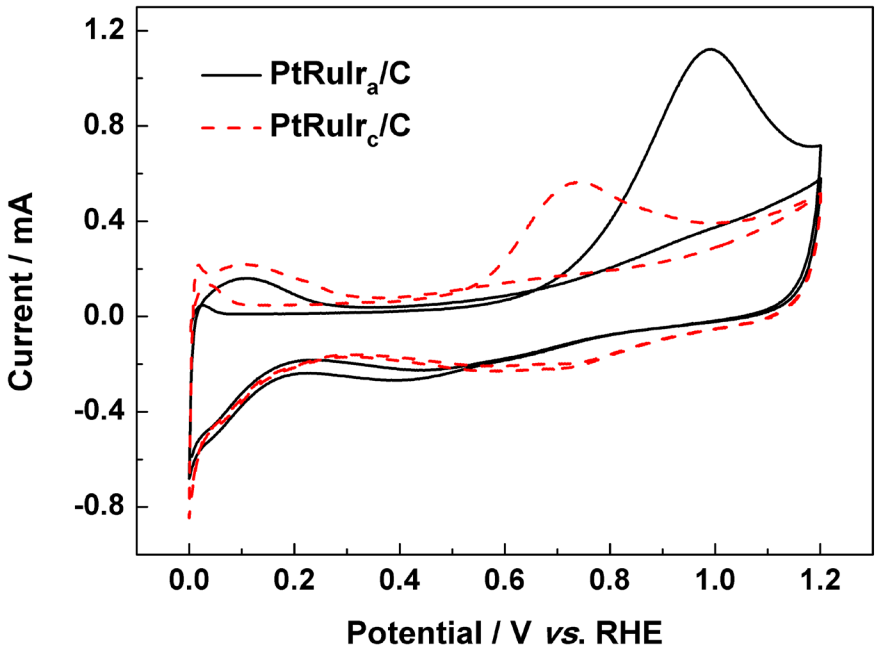

The electrocatalytic activity of $PtRuIr_c/C$ and $PtRuIr_a/C$ catalysts in methanol oxidation is shown in Figure 5. The onset potential and the activity for methanol oxidation on both catalysts are shown in Table 1. In the forward scan in Figure 5a, the current density (mass activity) of $PtRuIr_c/C$ (298 mA mg^{-1}) is 50% higher than that of $PtRuIr_a/C$ (147 mA mg^{-1}). In Figure 5b, the current density (specific activity) of the $PtRuIr_c/C$ is 3.6 times as large as that of $PtRuIr_a/C$. Although the particle size of $PtRuIr_c$ is obviously larger than that of $PtRuIr_a$, the $PtRuIr_c/C$ showed superior catalytic activity to $PtRuIr_a/C$, *i.e.*, lower onset potential, and higher oxidation current density due to the effect of the structure. Moreover, the mass and specific activities of $PtRuIr_c/C$ are distinctly higher than those of the $PtRuIr_a/C$ catalyst (see Table 1).

Figure 5. Cyclic voltammograms of $PtRuIr_c/C$ and $PtRuIr_a/C$ catalysts normalized to the metal loading on the electrodes (**a**) and $ECSA_{CO}$ (**b**), in 0.5 mol L^{-1} CH_3OH + 0.5 mol L^{-1} H_2SO_4 solution under N_2 atmosphere; scan rate = 50 mV s^{-1}.

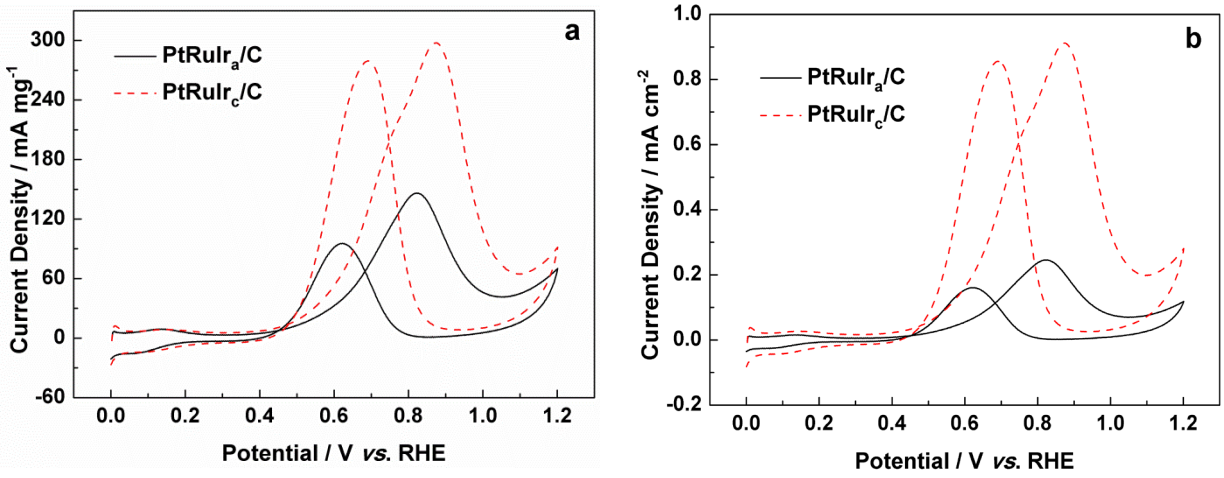

(**a**) (**b**)

Figure 6 shows the chronoamperometry curves for the $PtRuIr_c/C$ and $PtRuIr_a/C$ catalysts in 0.5 mol L^{-1} H_2SO_4 and 0.5 mol L^{-1} CH_3OH at a constant potential of 0.8 V (*vs*. RHE), the current density is normalized to the metal loading on the electrodes (a) and $ECSA_{CO}$ (b), respectively. Figure 6, shows that the potentiostatic current for all the catalysts initially decreased rapidly owing to the formation of CO_{ads} and other intermediate species during the methanol oxidation reaction. With time, the current density decayed more gradually and a pseudo-steady state was achieved. The decay can be attributed to the adsorbed anion SO_4^{2-} on the surface of the catalyst, thus restricting the methanol oxidation reaction. We calculated the long-term poisoning rate (δ) by measuring the linear decay of the current for a period of more than 500 s from Figure 6 by the following Equation (2) [33]:

$$\delta = \frac{100}{i_0} \times \left(\frac{di}{dt}\right)_{t>500} \quad (2)$$

where $\left(\frac{di}{dt}\right)_{t>500}$ is the slope of the linear portion of the current decay and i_0 is the current at the start of polarization back extrapolated from the linear current decay. The current densities of the $PtRuIr_c/C$ at 1000 s are 8.30 mA mg^{-1} and 0.025 mA cm^{-2}, while those of $PtRuIr_a/C$ catalysts at 1000 s are 4.0 mA mg^{-1} and 0.0067 mA cm^{-2}, respectively. The calculated δ values show that the poisoning rate 0.10 of the $PtRuIr_a/C$ catalysts is slow compared to 0.13 of the $PtRuIr_c/C$ catalyst. This indicates that the $PtRuIr_a/C$ catalyst had a relatively lower poisoning rate than the $PtRuIr_c/C$ catalyst. Thus, although the $PtRuIr_c/C$ catalyst had a larger $ECSA_{CO}$, the poisoning rate was faster than that of the $PtRuIr_a/C$ catalyst. This is probably because the faster and higher activities for the methanol oxidation reaction on the $PtRuIr_c/C$ electrode generated a larger amount of reactive intermediates and the ultimate poisoning species, rapidly producing the larger δ value.

3. Experimental Section

3.1. Preparation of PtRuIr/C Catalysts with Different Crystallinity

Amorphous PtRuIr/C catalyst ($PtRuIr_a/C$) was prepared by a modified organic colloid method in ethylene glycol (EG) solution. In a typical process, a $PtRuIr_a/C$ catalyst with a nominal weight Pt:Ru:Ir ratio of 3:3:1 was prepared as follows: 4.85 mL 20 mg mL^{-1} H_2PtCl_6·aqueous solutions, 1.99 mL 20 mg mL^{-1} $RuCl_3$, 2.56 mL 10 mg mL^{-1} H_2IrCl_6 and sodium citrate (220 mg) were dissolved in 30 mL ethylene glycol (EG) and stirred for 0.5 h. Pretreated carbon black Vulcan® XC72R (100 mg) was added to the mixture under stirring conditions. The pH of the system was adjusted to ~9 by drop-wise addition of a 5 wt % KOH/EG solution with vigorous stirring. The mixture was transferred to a flask and heated at 160 °C for 6 h and the resultant product was collected by filtration, washed with ultrapure water to remove all residual chloride ion, and then dried in air at 60 °C for 12 h. The metal loading is 20%. Crystalline PtRuIr/C catalyst ($PtRuIr_c/C$) was prepared by heating the above-prepared $PtRuIr_a/C$ powder in a tube furnace under H_2/N_2 atmosphere at 700 °C for 2 h.

Figure 6. Chronoamperometry curves of $PtRuIr_a/C$ and $PtRuIr_c/C$ catalysts for methanol oxidation, polarized at a constant potential of 0.6 V *vs*. Ag/AgCl at room temperature.

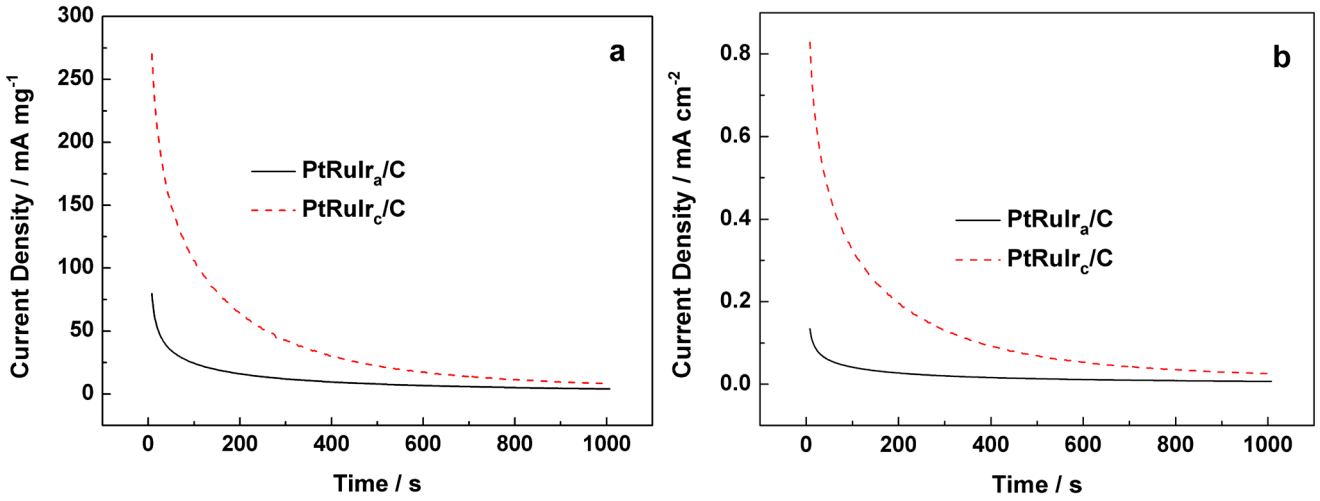

3.2. Measurements

The catalysts were characterized by recording their XRD patterns on a Shimadzu XD–3A (Japan), using filtered Cu-Kα radiation (λ = 0.15418 nm), generated at 40 kV and 30 mA. Scans for 2θ values were recorded at 4°/min between 10° and 90°. All X–ray diffraction patterns were analyzed using Jade 7.5 of Material Data, Inc. (MDI): peak profiles of individual reflections were obtained by a nonlinear least-square fit of the Cu-Kα corrected data. TEM measurements were carried out on a Tecnai G220 S–TWIN (FEI Company); the acceleration voltage was 200 kV. The average chemical compositions of the two catalysts were determined by the energy-dispersive X-ray spectroscopy (EDS) analysis and IRIS advantage inductively coupled plasma atomic emission spectroscopy (ICP-AES) system (Thermo Electron Corporation, America).

A common three-electrode cell was used for the electrochemical measurements, using a CHI 650D electrochemical work station. The counter and reference electrode were a platinum wire and an Ag/AgCl (3 M KCl) electrode, respectively, and the working electrode was a glassy carbon disk (5 mm in diameter). The thin-film electrode was prepared as follows: 5 mg of catalyst was dispersed ultrasonically in 1 mL Nafion/ethanol (0.25% Nafion) for 15 min. 8 μL of the dispersion was transferred onto the glassy carbon disk using a pipette, and then dried in the air. The metal loading on the film is 40.8 μg cm^{-2}.

4. Conclusions

Carbon-supported PtRuIr alloy catalysts of amorphous and crystalline structure were successfully synthesized and characterized. Electrochemical characterization found that although $PtRuIr_a$/C had a larger electrochemical surface area mainly due to the small size of the particles, the $PtRuIr_c$/C had the better electrochemical performance in the methanol oxidation reaction. However, the poisoning rate of the $PtRuIr_c$/C catalyst was faster than that on the $PtRuIr_a$/C catalyst. The difference in activity originates from the effect of the structure. Therefore, these results show that control of crystallinity of the active alloy nanoparticles can play an important role in both methanol oxidation activity and in the CO poisoning rate.

Acknowledgments

Thank you to the National Natural Science Foundation of China (21163018), the National Science Foundation for Post-Doctoral Scientists of China (20110490847, 2012T50587) and the research fund of the Key Laboratory of Fuel Cell Technology of Guangdong Province for financially supporting this work.

References

1. Peng, Z.; Yang, H. Designer platinum nanoparticles: Control of shape, composition in alloy, nanostructure and electrocatalytic property. *Nano Today* **2009**, *4*, 143–164.
2. Zhang, H.; Jin, M.; Xia, Y. Noble-Metal Nanocrystals with Concave Surfaces: Synthesis and Applications. *Angew. Chem. Int. Ed.* **2012**, *51*, 7656–7673.
3. Rabis, A.; Rodriguez, P.; Schmidt, T.J. Electrocatalysis for Polymer Electrolyte Fuel Cells: Recent Achievements and Future Challenges. *ACS Catal.* **2012**, *2*, 864–890.
4. An, X.-S.; Fan, Y.-J.; Chen, D.-J.; Wang, Q.; Zhou, Z.-Y.; Sun, S.-G. Enhanced activity of rare earth doped PtRu/C catalysts for methanol electro-oxidation. *Electrochim. Acta* **2011**, *56*, 8912–8918.
5. Daimon, H.; Kurobe, Y. Size reduction of PtRu catalyst particle deposited on carbon support by addition of non-metallic elements. *Catal. Today* **2006**, *111*, 182–187.
6. Gómez de la Fuente, J.L.; Martínez-Huerta, M.V.; Rojas, S.; Hernández-Fernández, P.; Terreros, P.; Fierro, J.L.G.; Peña, M.A. Tailoring and structure of PtRu nanoparticles supported on functionalized carbon for DMFC applications: New evidence of the hydrous ruthenium oxide phase. *Appl. Catal. B* **2009**, *88*, 505–514.

7. Huang, T.; Wang, X.Y.; Zhuang, J.H.; Cai, W.B.; Yu, A.S. Preparation of Porous PtRuCo Catalyst by One-Step Codeposition and Its Electrocatalytic Performance for Methanol Oxidation. *Electrochem. Solid State Lett.* **2009**, *12*, B112–B115.
8. Zhu, J.; Cheng, F.; Tao, Z.; Chen, J. Electrocatalytic Methanol Oxidation of $Pt_{0.5}Ru_{0.5-x}Sn_x$/C (x = 0−0.5). *J. Phys. Chem. C* **2008**, *112*, 6337–6345.
9. Liao, S.; Holmes, K.-A.; Tsaprailis, H.; Birss, V.I. High Performance PtRuIr Catalysts Supported on Carbon Nanotubes for the Anodic Oxidation of Methanol. *J. Am. Chem. Soc.* **2006**, *128*, 3504–3505.
10. Khorasani-Motlagh, M.; Noroozifar, M.; Ekrami-Kakhki, M.-S. Investigation of the nanometals (Ni and Sn) in platinum binary and ternary electrocatalysts for methanol electrooxidation. *Int. J. Hydrog. Energy* **2011**, *36*, 11554–11563.
11. Eguiluz, K.I. B.; Salazar-Banda, G.R.; Miwa, D.; Machado, S.A. S.; Avaca, L.A. Effect of the catalyst composition in the $Pt_x(Ru–Ir)_{1-x}$/C system on the electro-oxidation of methanol in acid media. *J. Power Sources* **2008**, *179*, 42–49.
12. Geng, D.S.; Matsuki, D.; Wang, J.J.; Kawaguchi, T.; Sugimoto, W.; Takasu, Y. Activity and Durability of Ternary PtRuIr/C for Methanol Electro-oxidation. *J. Electrochem. Soc.* **2009**, *156*, B397–B402.
13. Liang, Y.; Zhang, H.; Zhong, H.; Zhu, X.; Tian, Z.; Xu, D.; Yi, B. Preparation and characterization of carbon-supported PtRuIr catalyst with excellent CO-tolerant performance for proton-exchange membrane fuel cells. *J. Catal.* **2006**, *238*, 468–476.
14. Arico, A.S.; Bruce, P.; Scrosati, B.; Tarascon, J.-M.; van Schalkwijk, W. Nanostructured materials for advanced energy conversion and storage devices. *Nat. Mater.* **2005**, *4*, 366–377.
15. Qiao, Y.; Li, C.M. Nanostructured catalysts in fuel cells. *J. Mater. Chem.* **2011**, *21*, 4027–4036.
16. Loukrakpam, R.; Wanjala, B.N.; Yin, J.; Fang, B.; Luo, J.; Shao, M.; Protsailo, L.; Kawamura, T.; Chen, Y.; Petkov, V.; Zhong, C.-J. Structural and Electrocatalytic Properties of PtIrCo/C Catalysts for Oxygen Reduction Reaction. *ACS Catal.* **2011**, *1*, 562–572.
17. Cui, Z.; Kulesza, P.J.; Li, C.M.; Xing, W.; Jiang, S.P. Pd nanoparticles supported on HPMo-PDDA-MWCNT and their activity for formic acid oxidation reaction of fuel cells. *Int. J. Hydrog. Energy* **2011**, *36*, 8508–8517.
18. Wang, H.; Zhang, X.; Wang, R.; Ji, S.; Wang, W.; Wang, Q.; Lei, Z. Amorphous CoSn alloys decorated by Pt as high efficiency electrocatalysts for ethanol oxidation. *J. Power Sources* **2011**, *196*, 8000–8003.
19. Zhang, L.; Xia, D. Electrocatalytic activity of ordered intermetallic PtSb for methanol electro-oxidation. *Appl. Surf. Sci.* **2006**, *252*, 2191–2195.
20. Youn, D.H.; Han, S.; Bae, G.; Lee, J.S. Carbon-supported PtPb intermetallic compounds for electrooxidation of methyl formate. *Electrochem. Commun.* **2011**, *13*, 806–809.
21. Wang, H.; Wang, R.; Li, H.; Wang, Q.; Kang, J.; Lei, Z. Facile synthesis of carbon-supported pseudo-core@shell PdCu@Pt nanoparticles for direct methanol fuel cells. *Int. J. Hydrog. Energy* **2011**, *36*, 839–848.
22. Wang, H.; Linkov, V.; Ji, S.; Zhang, W.; Lei, Z.; Wang, R. Highly Active, Carbon-supported, PdSn Nano-core, Partially Covered with Pt, as Catalysts for Methanol Oxidation. *South Afr. J. Chem.* **2012**, *65*, 69–74.

23. Shrestha, S.; Liu, Y.; Mustain, W.E. Electrocatalytic Activity and Stability of Pt clusters on State-of-the-Art Supports: A Review. *Catal. Rev.* **2011**, *53*, 256–336.
24. Park, K.-W.; Choi, J.-H.; Kwon, B.-K.; Lee, S.-A.; Sung, Y.-E.; Ha, H.-Y.; Hong, S.-A.; Kim, H.; Wieckowski, A. Chemical and Electronic Effects of Ni in Pt/Ni and Pt/Ru/Ni Alloy Nanoparticles in Methanol Electrooxidation. *J. Phys. Chem. B* **2002**, *106*, 1869–1877.
25. Wang, R.; Jia, J.; Li, H.; Li, X.; Wang, H.; Chang, Y.; Kang, J.; Lei, Z. Nitrogen-doped carbon coated palygorskite as an efficient electrocatalyst support for oxygen reduction reaction. *Electrochim. Acta* **2011**, *56*, 4526–4531.
26. Gasteiger, H.A.; Markovic, N.; Ross, P.N.; Cairns, E.J. Methanol electrooxidation on well-characterized platinum-ruthenium bulk alloys. *J. Phys. Chem.* **1993**, *97*, 12020–12029.
27. Peng, Z.; Yang, H. Synthesis and Oxygen Reduction Electrocatalytic Property of Pt-on-Pd Bimetallic Heteronanostructures. *J. Am. Chem. Soc.* **2009**, *131*, 7542–7543.
28. Prabhuram, J.; Zhao, T.S.; Tang, Z.K.; Chen, R.; Liang, Z.X. Multiwalled Carbon Nanotube Supported PtRu for the Anode of Direct Methanol Fuel Cells. *J. Phys. Chem. B* **2006**, *110*, 5245–5252.
29. Zhou, C.; Wang, H.; Peng, F.; Liang, J.; Yu, H.; Yang, J. MnO_2/CNT Supported Pt and PtRu Nanocatalysts for Direct Methanol Fuel Cells. *Langmuir* **2009**, *25*, 7711–7717.
30. Mohamed, R.; Gouws, S.; Ferg, E. Characterization of Pt Catalysts for PEM Fuel Cells. *Mol. Cryst. Liquid Cryst.* **2012**, *555*, 149–157.
31. Schulenburg, H.; Durst, J.; Müller, E.; Wokaun, A.; Scherer, G.G. Real surface area measurements of Pt_3Co/C catalysts. *J. Electroanal. Chem.* **2010**, *642*, 52–60.
32. Jiang, J.; Kucernak, A. Electrooxidation of small organic molecules on mesoporous precious metal catalysts. I: CO and methanol on platinum. *J. Electroanal. Chem.* **2002**, *533*, 153–165.
33. Jiang, J.; Kucernak, A. Electrooxidation of small organic molecules on mesoporous precious metal catalysts. II: CO and methanol on platinum–ruthenium alloy. *J. Electroanal. Chem.* **2003**, *543*, 187–199.